Article

The Electronic Structure of the H-Cluster in the [FeFe]-Hydrogenase from *Desulfovibrio desulfuricans*: A Q-band Fe-ENDOR and HYSCORE Study

Alexey Silakov, Eduard J. Reijerse, Simon P. J. Albracht, E. Claude Hatchikian, and Wolfgang Lubitz

J. Am. Chem. Soc., **2007**, 129 (37), 11447-11458• DOI: 10.1021/ja072592s • Publication Date (Web): 28 August 2007

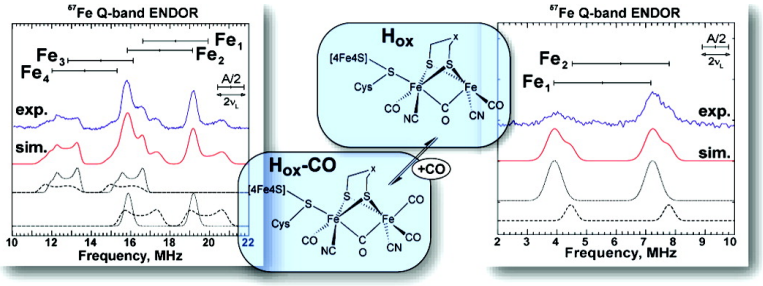

More About This Article

Additional resources and features associated with this article are available within the HTML version:

- Supporting Information
- Links to the 12 articles that cite this article, as of the time of this article download
- Access to high resolution figures
- Links to articles and content related to this article
- Copyright permission to reproduce figures and/or text from this article

View the Full Text HTML

J|A|C|S
ARTICLES
Published on Web 08/28/2007

The Electronic Structure of the H-Cluster in the [FeFe]-Hydrogenase from *Desulfovibrio desulfuricans*: A Q-band ^{57}Fe-ENDOR and HYSCORE Study

Alexey Silakov,[†] Eduard J. Reijerse,*[,†] Simon P. J. Albracht,[‡] E. Claude Hatchikian,[§] and Wolfgang Lubitz*[,†]

Contribution from the Max-Planck-Institut für Bioanorganische Chemie, Stiftstrasse 34-36, Mülheim a. d. Ruhr, 45470, Germany, Swammerdam Institute for Life Sciences, University of Amsterdam, Nieuwe Achtergracht 166, NL-1018 WV Amsterdam, The Netherlands, and Unité de Bioenergetique et Ingenierie des Proteines, Institut de Biologie Structural et Microbiologie, 31 Chemin Joseph Aiguier, F-13402 Marseille Cedex 20, France

Received April 13, 2007; E-mail: reijerse@mpi-muelheim.mpg.de; lubitz@mpi-muelheim.mpg.de

Abstract: The active site of the ^{57}Fe-enriched [FeFe]-hydrogenase (i.e., the "H-cluster") from *Desulfovibrio desulfuricans* has been examined using advanced pulse EPR methods at X− and Q-band frequencies. For both the active oxidized state (H_{ox}) and the CO inhibited form (H_{ox}-CO) all six ^{57}Fe hyperfine couplings were detected. The analysis shows that the apparent spin density extends over the whole H-cluster. The investigations revealed different hyperfine couplings of all six ^{57}Fe nuclei in the H-cluster of the H_{ox}−CO state. Four large ^{57}Fe hyperfine couplings in the range 20−40 MHz were found (using pulse ENDOR and TRIPLE methods) and were assigned to the $[4Fe-4S]_H$ (cubane) subcluster. Two weak ^{57}Fe hyperfine couplings below 5 MHz were identified using Q-band HYSCORE spectroscopy and were assigned to the $[2Fe]_H$ subcluster. For the H_{ox} state only two different ^{57}Fe hyperfine couplings in the range 10−13 MHz were detected using pulse ENDOR. An ^{57}Fe line broadening analysis of the X-band CW EPR spectrum indicated, however, that all six ^{57}Fe nuclei in the H-cluster are contributing to the hyperfine pattern. It is concluded that in both states the binuclear subcluster $[2Fe]_H$ assumes a $[Fe^{I}Fe^{II}]$ redox configuration where the paramagnetic Fe^{I} atom is attached to the $[4Fe-4S]_H$ subcluster. The ^{57}Fe hyperfine interactions of the formally diamagnetic $[4Fe-4S]_H$ are due to an exchange interaction between the two subclusters as has been discussed earlier by Popescu and Münck [Popescu, C.V.; Münck, E., *J. Am. Chem. Soc.* 1999, 121, 7877−7884]. This exchange coupling is strongly enhanced by binding of the extrinsic CO ligand. Binding of the dihydrogen substrate may induce a similar effect, and it is therefore proposed that the observed modulation of the electronic structure by the changing ligand surrounding plays an important role in the catalytic mechanism of [FeFe]-hydrogenase.

Introduction

Hydrogenases have been found in a wide variety of microorganisms, many of which are among the oldest in evolution.[1,2] Their general function is to catalyze one of the simplest redox reactions:

$$H_2 \rightleftharpoons 2H^+ + 2e^- \quad (1)$$

Three classes of hydrogenases have been identified over the last decades[2−4] and were classified according to their metal content. The active site of the [NiFe] class of hydrogenases[5−7] is characterized by a NiFe binuclear cluster in which the (redox) chemistry mainly occurs at the Ni atom.[8−12] The active site of the [FeFe] class (previously known as "Fe-only") contains six iron atoms arranged into a [4Fe−4S] cubane connected to a diatomic [2Fe] subcluster at which the hydrogen conversion is believed to occur.[13−17] A third class of hydrogenases was

[†] Max-Planck-Institut für Bioanorganische Chemie.
[‡] Swammerdam Institute for Life Sciences, University of Amsterdam.
[§] Unité de Bioenergetique et Ingenierie des Proteines, Institut de Biologie Structural et Microbiologie.

(1) Cammack, R.; Frey, M.; Robson, R. *Hydrogen as a Fuel. Learning from Nature*; Taylor & Francis Inc.: London, 2001.
(2) Vignais, P. M.; Billoud, B.; Meyer, J. *FEMS Microbiol. Rev.* **2001**, *25*, 455−501.
(3) Vignais, P. M.; Billoud, B. Occurrence and Classification of Hydrogenases: An Overview. *Chem. Rev.* **2007**. In press.
(4) Wu, L. F.; Mandrand, M. A. *FEMS Microbiol. Rev.* **1993**, *104*, 243−270.
(5) Volbeda, A.; Garcin, E.; Piras, C.; de Lacey, A. L.; Fernandez, V. M.; Hatchikian, E. C.; Frey, M.; Fontecilla-Camps, J. C. *J. Am. Chem. Soc.* **1996**, *118*, 12989−12996.
(6) Higuchi, Y.; Yagi, T.; Yasuoka, N. *Structure* **1997**, *5*, 1671−1680.
(7) Matias, P. M.; Soares, C. M.; Saraiva, L. M.; Coelho, R.; Morais, J.; Legall, J.; Carrando, M. A. *J. Biol. Inorg. Chem.* **2001**, *6*, 63−81.
(8) Albracht, S. P. J.; Kalkman, M. L.; Slater, E. C. *Biochim. Biophys. Acta* **1983**, *724*, 309−316.
(9) Lubitz, W.; Reijerse, E. J.; van Gastel, M. [NiFe] and [FeFe] Hydrogenase Studied by Advanced Magnetic Resonance Techniques. *Chem. Rev.* **2007**. In press.
(10) Lubitz, W.; van Gastel, M.; Gärtner, W. *Met. Ions Life Sci.* **2007**, *2*, 279−322.
(11) Best, S. *Coord. Chem. Rev.* **2005**, *249*, 1536−1554.
(12) Bleijlevens, B.; van Broekhuizen, F.; de Lacey, A. L.; Roseboom, W.; Fernandez, V. M.; Albracht, S. P. J. *J. Biol. Inorg. Chem.* **2004**, *9*, 743−752.

recently characterized. It contains a $Fe(CO)_2$ group bound to an organic cofactor. In this hydrogenase the iron center is probably not redox active[18] in contrast to [FeFe]-hydrogenases.

Some hydrogenases were found to be very active in H_2 production,[2,4,19,20] in particular the [FeFe] class. This has stimulated research on these enzymes with the aim to elucidate their structure and function to obtain a basis for a possible biohydrogen technology that provides a sustainable source of clean energy in the future.[1,21−23]

For the [FeFe]-hydrogenases from *Clostridium* (*C.*) *pasteurianum*[16] and *Desulfovibrio* (*D.*) *desulfuricans*[14] the X-ray crystallographic structures have been resolved. It was shown that the H-cluster consists of a novel binuclear iron subcluster ($[2Fe]_H$ subcluster) connected via a Cys-thiol to a classical cubane ($[4Fe-4S]_H$ subcluster). In addition to the H-cluster, the enzyme from *D. desulfuricans* also contains two classical [4Fe−4S] "cubanes" (so-called F-clusters), see Figure 1. The *C. pasteurianum* hydrogenase I also has these clusters, but in addition it contains a [4Fe−4S] cluster with a His ligand and a [2Fe−2S] cluster. The Fe−S clusters form the electronic path to the surface of the protein. Infrared spectroscopic studies[24,25] combined with the X-ray data suggest that each iron in the $[2Fe]_H$ subcluster is coordinated by the diatomic ligands CO and CN^-. The distal iron (Fe_d) of the enzyme in the H_{ox} state has one vacant (exchangeable) site. The bridging dithiol ligand was originally described as $HS-(CH_2)_3-SH$ (1,3-propanedithiolate).[14] DFT calculations aimed to elucidate the catalytic function of the H-cluster[26,27] as well as a reanalysis of the X-ray data,[28] suggested, however, that the central atom could be a nitrogen, i.e., $HS-CH_2-NH-CH_2-SH$ (di(thiomethyl)amine).

The enzymes from *C. pasteurianum* and *Megasphaera (M.) elsdenii* are very oxygen sensitive and must be purified under strict anaerobic conditions.[30,31] In contrast, the hydrogenases from *D. desulfuricans* and *D. vulgaris* Hildenborough (that have identical primary structures[32]) can be isolated aerobically,[33] but in this case the enzyme is inactive and needs to be activated under reducing conditions (e.g., with H_2).

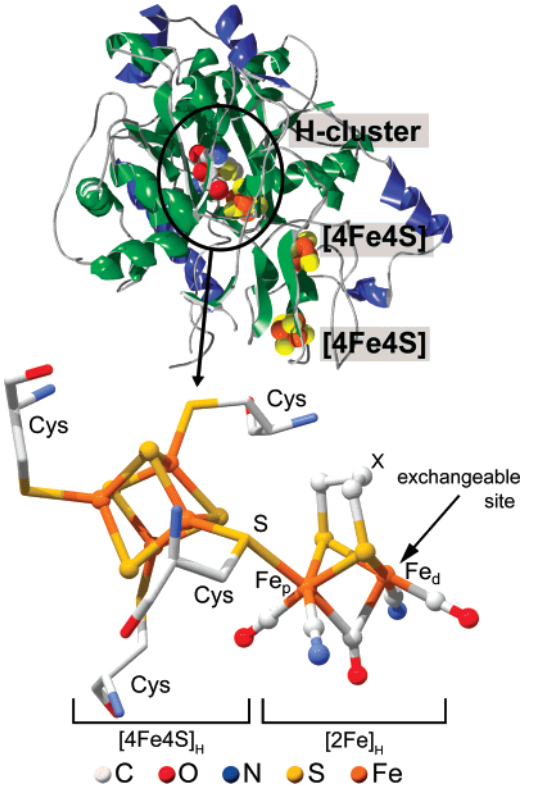

Figure 1. Structure of the [FeFe]-hydrogenase from *D. desulfuricans* (top) and the active site (H-cluster) in the active oxidized state (bottom). The coordinates of the protein structure were taken from the crystal structure published by Nicolet et al.[28] (Protein Data Bank entry 1HFE). Coordinates of the H-cluster were combined from structures of the [FeFe]-hydrogenase from *D. desulfuricans*[28] and *C. pasteurianum* (hydrogenase I, Protein Data Bank entry 1C4A).[16] Note that Fe_p is six-coordinate, whereas Fe_d has five ligands in the H_{ox} state.[13] The open coordination (exchangeable) site is occupied by CO in the inhibited H_{ox}−CO state. Both H_{ox} and H_{ox}−CO are paramagnetic[29] and studied in this work.

The reductive activation of [FeFe]-hydrogenase from *D. vulgaris* Hildenborough has been investigated in detail by Patil et al. using X-band CW EPR spectroscopy and mediated electrochemistry.[34] The same process has also been studied using Mössbauer[35] and infrared spectroscopy.[36] In the aerobically purified enzyme the H-cluster is in a double oxidized form (H_{ox}^{air}) and reveals no EPR signal (see Scheme 1). The observed weak, almost isotropic, EPR signal at $g = 2.02$ is attributed to a fraction of F-clusters ([4Fe−4S]) which are converted to $[3Fe4S]^{1+}$ clusters by oxidative damage. During the reductive activation of the enzyme (Scheme 1) a rhombic signal appears (for *D. vulgaris* at $g = 2.06, 1.96, 1.89$) with a maximum intensity at about −110 mV (vs NHE).[34] This signal is believed

(13) Nicolet, Y.; Lemon, B. J.; Fontecilla-Camps, J. C.; Peters, J. W. *Trends Biochem. Sci.* **2000**, *25*, 138−143.
(14) Nicolet, Y.; Piras, C.; Legrand, P.; Hatchikian, C. E.; Fontecilla-Camps, J. C. *Structure* **1999**, *7*, 13−23.
(15) Nicolet, Y.; Cavazza, C.; Fontecilla-Camps, J. C. *J. Inorg. Biochem.* **2002**, *91*, 1−8.
(16) Peters, J. W.; Lanzilotta, W. N.; Lemon, B. J.; Seefeldt, L. C. *Science* **1998**, *282*, 1853−1858.
(17) Lemon, B. J.; Peters, J. W. *Biochemistry* **1999**, *38*, 12969−12973.
(18) Shima, S.; Lyon, E. J.; Thauer, R. K.; Mienert, B.; Bill, E. *J. Am. Chem. Soc.* **2005**, *127*, 10430−10435.
(19) Cammack, R. *Nature* **1999**, *397*, 214−215.
(20) Hatchikian, E. C.; Forget, N.; Fernandez, V. M.; Williams, R.; Cammack, R. *Eur. J. Biochem.* **1992**, *209*, 357−365.
(21) Miyake, J., Igarashi, Y., Rögner, M., Eds. *Biohydrogen III*; Elsevier: Amsterdam, 2004.
(22) Photohydrogen. In *Artificial Photosynthesis, Part IV*; Collings, A. F., Critchley, C., Eds.; Wiley-VCH Verlag: Weinheim, 2007; pp 211−240.
(23) Pace, R. J. An Integrated Artificial Photosynthesis Model. In *Artificial Photosynthesis: From Basic Biology to Industrial Application*; Collings, A. F., Critchley, C., Eds.; Wiley-VCH Verlag: Weinheim, 2005; pp 13−34.
(24) Chen, Z. J.; Lemon, B. J.; Huang, S.; Swartz, D. J.; Peters, J. W.; Bagley, K. A. *Biochemistry* **2002**, *41*, 2036−2043.
(25) Pierik, A. J.; Hulstein, M.; Hagen, W. R.; Albracht, S. P. J. *Eur. J. Biochem.* **1998**, *258*, 572−578.
(26) Fan, H. J.; Hall, M. B. *J. Am. Chem. Soc.* **2001**, *123*, 3828−3829.
(27) Georgakaki, I. P.; Thomson, L. M.; Lyon, E. J.; Hall, M. B.; Darensbourg, M. Y. *Coord. Chem. Rev.* **2003**, *238*, 255−266.
(28) Nicolet, Y.; de Lacey, A. L.; Vernede, X.; Fernandez, V. M.; Hatchikian, E. C.; Fontecilla-Camps, J. C. *J. Am. Chem. Soc.* **2001**, *123*, 1596−1601.
(29) Albracht, S. P. J.; Roseboom, W.; Hatchikian, C. *J. Biol. Inorg. Chem.* **2006**, *11*, 88−101.
(30) Chen, J. S.; Mortenson, L. E. *Biochim. Biophys. Acta* **1974**, *371*, 283−298.
(31) Vandijk, C.; Mayhew, S. G.; Grande, H. J.; Veeger, C. *Eur. J. Biochem.* **1979**, *102*, 317−330.
(32) Hatchikian, E. C.; Magro, V.; Forget, N.; Nicolet, Y.; Fontecilla-Camps, J. C. *J. Bacteriol.* **1999**, *181*, 2947−2952.
(33) Hagen, W. R.; Vanberkelarts, A.; Krusewolters, K. M.; Voordouw, G.; Veeger, C. *FEBS Lett.* **1986**, *203*, 59−63.
(34) Patil, D. S.; Moura, J. J. G.; He, S. H.; Teixeira, M.; Prickril, B. C.; Dervartanian, D. V.; Peck, H. D.; Legall, J.; Huynh, B. H. *J. Biol. Chem.* **1988**, *263*, 18732−18738.
(35) Pereira, A. S.; Tavares, P.; Moura, I.; Moura, J. J. G.; Huynh, B. H. *J. Am. Chem. Soc.* **2001**, *123*, 2771−2782.
(36) Roseboom, W.; de Lacey, A. L.; Fernandez, V. M.; Hatchikian, C.; Albracht, S. P. J. *J. Biol. Inorg. Chem.* **2006**, *11*, 102−118.

Scheme 1

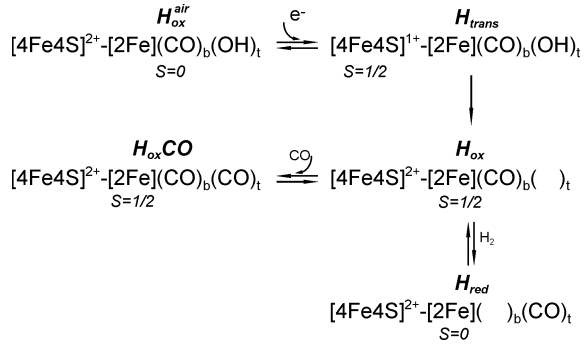

to belong to the H-cluster (the so-called "H_{trans}" state). However, since the characteristic *g*-values are similar to the ones observed for an $[4Fe-4S]^{1+}$ cluster, it was concluded that this state is characterized by reduction of the $[4Fe-4S]_H$ subcluster. Upon lowering the redox potential further, this signal is replaced by another rhombic signal with *g*-values of $g = 2.10, 2.04, 2.00$. This is the characteristic signal observed in almost all [FeFe]-hydrogenases and is assigned to the "oxidized" form of the H-cluster in the active enzyme (H_{ox} state). It differs fundamentally from EPR spectra of classical [4Fe−4S] clusters. During the reductive titration experiments of Patil et al.[34] the intensity of the rhombic signal was maximized at a potential of about −300 mV. Below −320 mV, this signal rapidly decreases. Under 1 bar of H_2 the H-cluster is EPR silent (H_{red} state). Another quite complex EPR signal is obtained with a maximum intensity at −350 mV. This signal is assigned to the two dipolar-coupled reduced F-clusters $[4Fe-4S]^{1+}$ of the electron transport chain (see Figure 1). In Scheme 1 a summary is presented of the various states of the H-cluster.

All [FeFe]-hydrogenases are very sensitive to inhibition by CO. The external CO ligand is coordinated to the vacant (exchangeable) site at Fe_d in the H-cluster[17] see Figure 1. Binding of CO to the enzyme in the H_{ox} state causes a change of the EPR signal. An axial EPR spectrum is observed ($g_\perp = 2.006$, $g_{||} = 2.065$), which is indicative of the "H_{ox}−CO" state. From EPR and infrared investigations it is known that upon light excitation at temperatures between 20 and 70 K the external CO ligand can be (reversibly) removed and the original EPR signal of the H_{ox} state is restored.[25,29,36,37] Mössbauer and EPR investigations of ^{57}Fe-enriched [FeFe]-hydrogenases I and II from *C. pasteurianum*[38−41] showed that inhibition of the H_{ox} state by CO leads to a large change of the electronic structure. It was found that, despite the fact that only one unpaired electron is present in the system, the iron nuclei of both parts of the H-cluster experience a hyperfine interaction. Popescu and Münck[38] have shown that the $[4Fe-4S]_H$ subcluster remains in the [2+] state in all relevant states of the H-cluster (except for H_{trans}). They concluded that the irons of the binuclear cluster are in the $[Fe^{II}Fe^{III}]_H$ oxidation state for H_{ox} and in the $[Fe^{II}Fe^{II}]_H$ state for H_{red}. However, DFT calculations on model systems[42,43] suggest other valencies of the irons in the $[2Fe]_H$ subcluster; the fully oxidized, inactive state (H_{ox}^{air}) is believed to be $Fe^{II}Fe^{II}$, the H_{ox} state is $Fe^{II}Fe^{I}$, and the H_{red} state is Fe^{I}-Fe^{I}. Later, Pereira et al.[35] used Mössbauer spectroscopy for the investigation of the [FeFe]-hydrogenase from *D. vulgaris* Hildenborough. For this H-cluster ^{57}Fe hyperfine coupling values were obtained similar to the ones found for the *C. pasteurianum* hydrogenase II by Popescu and Münck.[38]

The main purpose of the current study is to gain more specific information about the electronic structure of the EPR accessible states (H_{ox} and H_{ox}−CO) of the H-cluster through a detailed investigation of its ^{57}Fe hyperfine interactions. Furthermore, our study aims to finally determine the formal oxidation states of all iron atoms of the paramagnetic states of the H-cluster and also deduce those of the intermediate EPR-silent states. This is of key importance for a detailed understanding of the catalytic site of the [FeFe]-hydrogenase and for the hydrogen conversion mechanism.

In the present work pulse EPR, electron nuclear double resonance (ENDOR), and electron spin−echo envelope modulation (ESEEM) techniques were used at Q-band frequencies in addition to the conventional X-band to gain higher resolution and sensitivity and to disentangle the complicated ^{57}Fe hyperfine spectra. It is demonstrated that the ^{57}Fe hyperfine tensor components can be determined with high accuracy, thus facilitating the comparison between different [FeFe]-hydrogenases and providing reference data for further theoretical investigations, i.e., quantum chemical calculations. The exchange-coupling model of the H-cluster is discussed. The detailed analysis of our data together with recent theoretical[44] and spectroscopic[29,35,36,38] studies of the H-cluster finally allow the assignment of the spin and oxidation states of the iron atoms in the catalytic $[2Fe]_H$ site.

Materials and Methods

Sample Preparation. The enzyme was purified from *D. desulfuricans* cells as described.[20] Quantitative amino acid analysis has been used for protein determination. The enzyme concentration derived in this way was in excellent agreement with the concentrations determined from the Fe−S signals in the H_2-reduced enzyme.[29,36] For the ^{57}Fe-enriched enzyme (enrichment, ≥90%),[29] the bulk salts for the growth medium were depleted of Fe by passage over Chelex-100, and the medium was supplemented with ^{57}Fe. The non-enriched enzyme was purified aerobically using the procedure described by Pierik et al.[45]The enzyme was activated by incubation under H_2 for 10 min and oxidized in the activated form by replacing H_2 by Ar. After preparation, the samples were transferred to quartz tubes (outer diameter of 3 mm and inner of 2 mm) and were then frozen and stored in liquid nitrogen.

Pulse EPR methods. Most of the results presented here have been obtained by pulse EPR methods. Figure 2 summarizes the pulse sequences, used in this study. In some cases the EPR spectra were obtained by integration over the free induction decay (FID) created by a single soft microwave $\pi/2$ pulse ($t_{mw} = 500-1000$ ns, see Figure 2A). FID detection was used instead of conventional detection of electron spin−echo (ESE), since the ESE intensity was strongly affected by field-dependent nuclear (^{57}Fe and ^{14}N) modulation. This method produces EPR spectra comparable to those of CW EPR.

(37) Patil, D. S.; Huynh, B. H.; He, S. H.; Peck, H. D.; Dervartanian, D. V.; Legall, J. *J. Am. Chem. Soc.* **1988**, *110*, 8533−8534.
(38) Popescu, C. V.; Münck, E. *J. Am. Chem. Soc.* **1999**, *121*, 7877−7884.
(39) Wang, G.; Benecky, M. J.; Huynh, B. H.; Cline, J. F.; Adams, M. W. W.; Mortenson, L. E.; Hoffman, B. M.; Münck, E. *J. Biol. Chem.* **1984**, *259*, 4328−4331.
(40) Telser, J.; Benecky, M. J.; Adams, M. W. W.; Mortenson, L. E.; Hoffman, B. M. *J. Biol. Chem.* **1986**, *261*, 3536−3541.
(41) Telser, J.; Benecky, M. J.; Adams, M. W. W.; Mortenson, L. E.; Hoffman, B. M. *J. Biol. Chem.* **1987**, *262*, 6589−6594.
(42) Cao, Z. X.; Hall, M. B. *J. Am. Chem. Soc.* **2001**, *123*, 3734−3742.
(43) Liu, Z. P.; Hu, P. *J. Am. Chem. Soc.* **2002**, *124*, 5175−5182.
(44) Fiedler, A. T.; Brunold, T. C. *Inorg. Chem.* **2005**, *44*, 9322−9334.
(45) Pierik, A. J.; Hagen, W. R.; Redeker, J. S.; Wolbert, R. B. G.; Boersma, M.; Verhagen, M. F. J. M.; Grande, H. J.; Veeger, C.; Mutsaers, P. H. A.; Sands, R. H.; Dunham, W. R. *Eur. J. Biochem.* **1992**, *209*, 63−72.

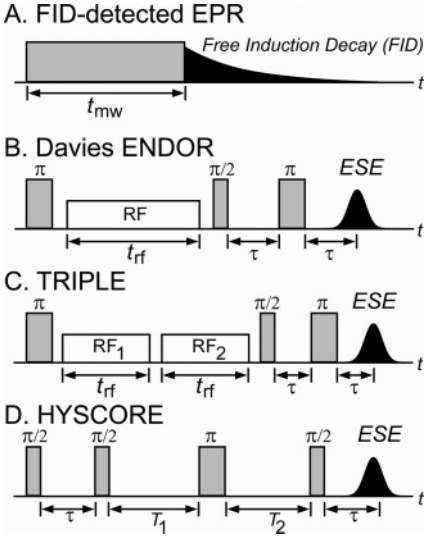

Figure 2. EPR pulse sequences, used in this study: (A) FID detected EPR. The length of the MW pulse (t_{mw}) is fixed, and the external magnetic field is varied. (B) Davies ENDOR sequence. The frequency of the RF pulse is varied. (C) TRIPLE sequence. In order to obtain a 1D spectrum, the frequency of the RF pulse RF_1 is scanned, while the frequency of the pulse RF_2 is fixed. (D) HYSCORE sequence. The delay between the first and second MW pulse (τ) is fixed, while delays T_1 and T_2 are varied. In this sequence, a four-step phase cycling of the last two MW pulses is used.

Electron nuclear double resonance (ENDOR)[46] has been used for studying the ^{57}Fe hyperfine interactions. In our investigation we used the pulse sequence (Figure 2B) established by Davies in 1974[47] (so-called "Davies ENDOR"). The excitation of nuclear spin transitions is detectable through a reduction of the electron spin−echo intensity. The length of the RF pulse was adjusted to maximize the ENDOR effect of the most prominent feature in the ENDOR spectrum.

The TRIPLE (sometimes called double ENDOR) sequence has been used for determining the relative signs of the hyperfine couplings, obtained from Davies ENDOR experiments. In this study the TRIPLE sequence was derived from the regular Davies ENDOR pulse sequence, where two RF π pulses are applied instead of one[48] (Figure 2C). A one-dimensional (1D) TRIPLE spectrum is obtained by sweeping one of the RF pulses over the ENDOR spectral range, while the other one has a fixed frequency, in resonance with one of the nuclear spin transitions. In this contribution "difference TRIPLE" spectra are presented, obtained by subtraction of the TRIPLE spectrum from a reference ENDOR spectrum.

Weak ^{57}Fe hyperfine couplings (<5 MHz) were detected using hyperfine sublevel correlation spectroscopy (HYSCORE). This is a two-dimensional (2D) four-pulse ESEEM experiment,[49] which allows the detection of correlations between ESEEM frequencies belonging to different electron spin manifolds of the same nuclear spin (Figure 2D). To suppress the effects of unwanted echoes, a four-step phase cycling of the MW pulses is used.[50] The time-domain HYSCORE spectra were processed using third-order background polynomial subtraction and hamming apodization followed by 2D fast Fourier transformation (2D-FFT).

Experimental Setup. All pulse Q-band measurements were performed on a Bruker ELEXSYS E-580 Q-band spectrometer with the SuperQ-FT microwave bridge. The solid-state microwave amplifier in this bridge produces a power of 0.5 W at the resonator, which is sufficient for obtaining a MW $\pi/2$ pulse of 32 ns. For these measurements we used a home-built slightly overcoupled cylindrical TE_{011} resonator[51] with a construction similar to the one described by Sienkiewicz et al.[52] Cryogenic temperatures (10−20 K) were reached using an Oxford CF935 flow cryostat.

The long radio frequency (RF) pulses needed for Q-band ^{57}Fe ENDOR and TRIPLE, (>45 μs) were found to cause heating in the resonator, whereby the physical properties of the resonator are changed, especially in case of high repetition rates. These effects lead to changes in intensity of the ESE signal that are not correlated with the ENDOR effect and give rise to artifacts and baseline distortions in the ENDOR spectra. In order to avoid such effects a random-acquisition procedure has been used, in which the RF frequency is stochastically varied in the frequency range of the experiment. In this case the time-dependent heating effects are randomized and only add to the experimental noise.[53]

For pulse ENDOR experiments with the random-acquisition procedure we used a home-built data acquisition system, based on *SpecMan* software on a personal computer.[53] The Bruker spectrometer was used for generating MW pulses and triggering the *SpecMan* system, which in turn controls the generation of RF pulses and records the signal coming from the Bruker spectrometer. In these experiments the RF pulses were generated by an Agilent E4420B radio frequency generator and amplified either by an ENI 3200L RF solid-state amplifier, (300 W, 55 dB gain) or by an ENI A-500 RF amplifier (500 W, 60 dB gain). In order to suppress the "harmonics" of the ^{1}H ENDOR signals (around 51 MHz at 1.2 T), a Trilithic high-power low-pass filter H4LE35-3-AA (cutoff frequency ~35 MHz) was used.

The TRIPLE resonance experiments were also performed using the *SpecMan* system. All TRIPLE spectra were obtained in one 2D experiment (overall five traces). For one of the traces the second RF pulse was set to a nonresonant frequency of 25 MHz. This trace is identical to the ENDOR spectrum and therefore was used as a reference to obtain the four "difference TRIPLE" spectra.

In this case a Rohde and Schwarz SMT02 continuous-wave RF generator with a Mini-Circuits ZASWA-2-50DR switch was added to generate the fixed-frequency pumping RF pulse.

The X-band ENDOR measurements were performed on a Bruker ELEXSYS E-580 X-band spectrometer with a SuperX-FT microwave bridge and an CF935 Oxford flow cryostat in the temperature range 10−20 K. An overcoupled Bruker ER 4118X-MD5-EN dielectric ring ENDOR resonator was used for these experiments. The MW pulses were amplified by using either a Traveling Wave Tube (TWT) amplifier (1 kW) or the Bruker AmpX10 solid-state amplifier (10 W). In order to suppress the harmonics of the ^{1}H ENDOR signals, a low-pass Trilithic filter H5LEC10-3-AA with cutoff frequency at 10 MHz was used. The X-band ENDOR spectra were recorded using the standard Bruker data acquisition software. Due to the relatively short RF pulses (10−15 μs) and slow repetition rate the use of the random scan acquisition had only a minor effect on the background of the ENDOR spectra and was therefore not used. The X-band cw EPR spectra presented here have been measured using a critically coupled Bruker ER4118X-MS3-W1 split-ring resonator.

Spectral Simulations. The interpretation of the pulse EPR experimental data was facilitated using home-written simulation programs in MATLAB 6.5.[54] We used the following spin Hamiltonian for obtaining the energy levels and their wavefunctions for simulations of the HYSCORE and ENDOR spectra:[55]

(46) Feher, G. *Phys. Rev.* **1956**, *103*, 834−835.
(47) Davies, E. R. *Phys. Lett. A* **1974**, *A 47*, 1−2.
(48) Mehring, M.; Hofer, P.; Grupp, A. *Ber. Bunsen-Ges. Phys. Chem.* **1987**, *91*, 1132−1137.
(49) Hofer, P.; Grupp, A.; Nebenfuhr, H.; Mehring, M. *Chem. Phys. Lett.* **1986**, *132*, 279−282.
(50) Gemperle, C.; Aebli, G.; Schweiger, A.; Ernst, R. R. *J. Magn. Reson.* **1990**, *88*, 241−256.
(51) Sinnecker, S.; Reijerse, E.; Neese, F.; Lubitz, W. *J. Am. Chem. Soc.* **2004**, *126*, 3280−3290.
(52) Sienkiewicz, A.; Smith, B. G.; Veselov, A.; Scholes, C. P. *Rev. Sci. Instrum.* **1996**, *67*, 2134−2138.
(53) Epel, B.; Gromov, I.; Stoll, S.; Schweiger, A.; Goldfarb, D. *Concepts Magn. Reson., Part B* **2005**, *26B*, 36−45.
(54) *MATLAB 6.5*, Mathworks, 2002.
(55) Abragam, A.; Bleaney, B. *Electron Paramegnetic Resonance of transition ions*; Clarendon Press: Oxford, 1970.

$$\hat{H}_0 = \beta\vec{B}\cdot\mathbf{g}\cdot\hat{S} + \sum_{i=1}^{n}(-\beta_n g_n^i \vec{B}\cdot\hat{I}_i + \hat{S}\cdot\mathbf{A}\cdot\hat{I}_i) \qquad (2)$$

where β is the Bohr magneton, β_n the nuclear magneton, g_n^i is the g-factor of ith nucleus, and g represents the electronic **g** tensor. The first and second terms in the expression correspond to the electron and nuclear Zeeman interactions with the external magnetic field $\vec{B}$; the third term describes the hyperfine interaction defined by tensor **A**. The H-cluster reveals an $S = {}^1/_2$ electronic ground state for both investigated species. Since this work concerns investigation of the ^{57}Fe hyperfine interactions, the nuclear spin (I) in our simulations is $I(^{57}\text{Fe}) = 1/2$ and $g_n(^{57}\text{Fe}) = 0.1806$. In all calculations, the electron Zeeman interaction was assumed to be the dominant term, which is a good approximation for both the X- and Q-band frequency ranges. All other interactions were treated as a perturbation. The orientation of the hyperfine interaction tensors was defined with respect to the principal axes of the electronic **g** tensor. In this study we use the y-convention for rotation according to the Euler angles (φ, θ, ψ). In this convention the first rotation is by angle φ about the z-axis, the second is by angle θ about the new y'-axis and the third is by angle ψ about the new z''-axes.[56] The ENDOR signals of each nucleus were calculated separately and then summed with appropriate weighting coefficients.

HYSCORE simulations were performed using the general expression for the intensity of the electron spin−echo after applying the HYSCORE sequence with ideal pulses, described by Shane et al.[57] First, calculations of the frequencies and amplitudes of the cross-peaks were performed in the frequency domain. Then, the calculated 2D spectra were transferred to the time domain using the inverse discrete Fourier transformation. After elimination of the negative time parts and simulation of lineshapes (based on Gaussian line shape) the time-domain data were transformed back to the frequency domain.

Simulations of the CW EPR spectra were performed by EasySpin[58]-based programs, written in MatLab.[54] The alignment of the local axes of the hyperfine tensors to the structure of the H-cluster in the H_{ox}−CO state was facilitated using a home-written program in MATLAB 6.5.[54] The atomic coordinates were taken from the geometry-optimized structure of the H-cluster in the H_{ox}−CO state, presented by Fiedler et al.[44]

Results

EPR Spectra. Figure 3 shows the Q-band FID (free induction decay) detected EPR spectra of the active oxidized state (H_{ox}) and the CO inhibited state (H_{ox}−CO) of the nonenriched enzyme recorded at 15 K. To facilitate a comparison with the CW EPR spectra the first derivative spectra (pseudomodulated[59]) are shown. The Q-band measurements of the FID-detected EPR spectrum of the H_{ox}−CO sample show a slight rhombic distortion of the axial signal. We have found the following characteristic g-values for the EPR spectrum of the H_{ox}−CO state of the H-cluster (see also Table 1): $g_1 = 2.065$, $g_2 = 2.007$, $g_3 = 2.001$ (error ± 0.001). The H_{ox} state shows the well-known rhombic EPR spectrum ($S = {}^1/_2$) characterized by the principal g-values: $g_1 = 2.100$, $g_2 = 2.040$, $g_3 = 1.999$ (error ± 0.001). The H_{ox} spectrum contains some contribution from the spectrum of the reduced dipolar-coupled F-clusters as well as a signal similar to the H_{ox}−CO spectrum.[29] This contribution points to a possible partial damage of the protein during the aerobic isolation. Albracht et al. have recently shown that oxidative and light damage of the active enzyme leads to a kind of cannibalization among the H-clusters in which the released CO ligands of damaged H-clusters are captured by intact ones which in turn are getting inhibited, leading to the formation of a stable H_{ox}−CO state.[29,36]

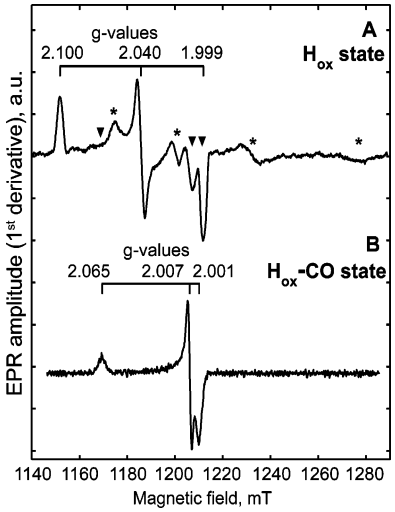

Figure 3. First derivative of the Q-band FID detected EPR spectra of [FeFe]-hydrogenase of *D. desulfuricans* in the H_{ox} (top) and the H_{ox}−CO (bottom) state, obtained by pseudomodulation of the original spectra. Experimental conditions: temperature, 15 K; microwave frequency 33.86 GHz; microwave pulse length (t_{mw}), 400 ns. The Q-band spectra of the nonenriched H_{ox}−CO state reveal a small but distinct rhombicity of the EPR signal. The estimated g-values for the spectrum of the H_{ox} and the H_{ox}−CO state are given (error ± 0.001). Triangles and stars in the spectrum A indicate overlapping signals resulting from the presence of the H_{ox}−CO state (▼) (about 20%), and reduced dipolar-coupled F-clusters (*).

Table 1. Comparison of g-Values of the H_{ox} and the H_{ox}−CO States of Different Enzymes

	H_{ox}			H_{ox}−CO			
enzyme	g_1	g_2	g_3	g_1	g_2	g_3	ref
D. desulfuricans	2.100	2.040	1.999	2.065	2.007	2.001	*a*
C. pasteurianum, hydrogenase I	2.10	2.04	2.00	2.07	2.01	2.01	70
C. pasteurianum, hydrogenase II	2.078	2.027	1.999	2.032	2.017	1.997	41

[a] This study.

^{57}Fe Hyperfine Couplings of the H_{ox}−CO State. The Q-band ^{57}Fe orientation-selective Davies ENDOR spectra for the H_{ox}−CO state at different field positions are shown in Figure 4B. In the present case of strong hyperfine interaction ($|A| > |2\nu_n|$), the ENDOR signals appear as doublets centered at $|A/2|$, and split by twice the Larmor frequency ν_{Fe} ($\nu_{Fe} = 1.652$ MHz at 1200 mT and 0.468 MHz at 340 mT) according to the resonance conditions:

$$\nu_{ENDOR} = |A/2 \pm \nu_{Fe}| \qquad (3)$$

Several of these (partly overlapping) doublets can be recognized in the orientation selective ENDOR spectra. As indicated by the simulations four different sets of anisotropically broadened doublets have been identified. The simulation parameters are summarized in Table 2 (A_1^{CO}−A_4^{CO}). As can be seen in Figure 4A, the obtained simulation parameters also reproduce the X-band Davies ENDOR spectrum (measured at $g = 2.007$) very well. The X-band ^{57}Fe ENDOR spectrum shows a good

(56) Schweiger, A.; Jeschke, G. *Principles of Pulse Electron Paramagnetic Resonance*; Oxford University Press: New York, 2001.
(57) Shane, J. J.; Hofer, P.; Reijerse, E. J.; de Boer, E. *J. Magn. Reson.* **1992**, *99*, 596−604.
(58) Stoll, S. *J. Magn. Reson.* **2005**, *177*, 390−403.
(59) Hyde, J. S.; Pasenkiewicz-Gierula, W.; Jesmanowicz, A.; Antholine, W. E. *Appl. Magn. Reson.* **1990**, *1*, 483−496.

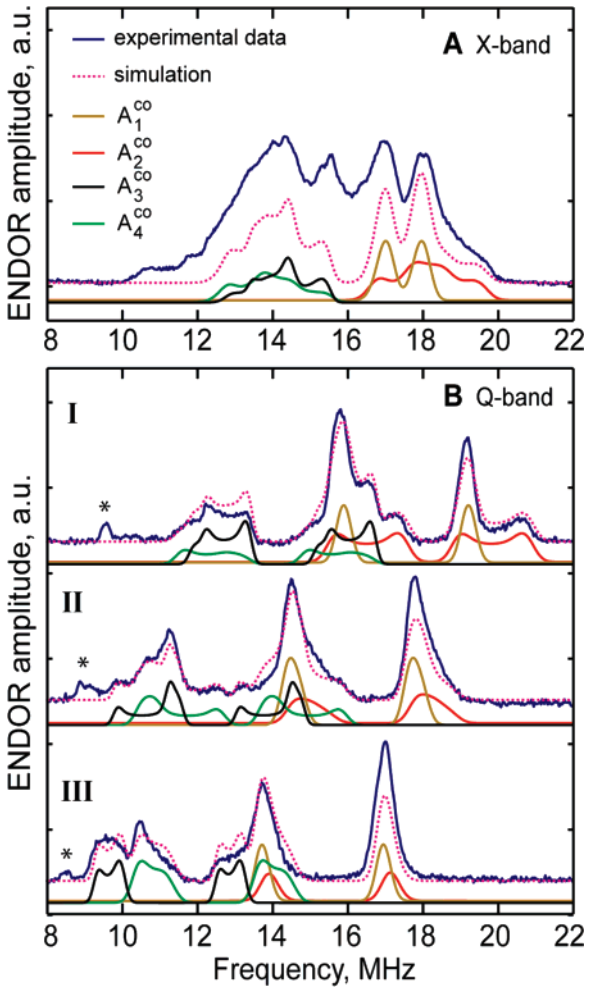

Figure 4. X- and Q-band Davies ENDOR spectra of the ^{57}Fe-enriched [FeFe]-hydrogenase of *D. desulfuricans* in the H_{ox}−CO state. (A) X-band Davies ENDOR spectrum, recorded at $T = 15$ K with $t_{rf} = 7$ μs RF pulse. The magnetic field was set to 345 mT ($B_0||g_2$). Note that the ^{57}Fe-ENDOR signals are overlapping with the ENDOR spectrum of protons ($\nu(^1H) =$ 14.68 MHz at 345 mT); (B) Q-band Davies ENDOR spectra, recorded at $T = 15$ K with $t_{rf} = 45$ μs RF pulse (optimized on the ENDOR signals around 16 MHz at $g = 2.007$) at a magnetic field of (I) 1205.4 mT; (II) 1185.0 mT; (III) 1173.0 mT; microwave frequency, 33.884 GHz. The blue solid lines represent the experimental data. The dotted magenta lines represent simulations of the ENDOR spectra. The colored solid lines below each experimental spectrum are the components of the simulation corresponding to the four HF couplings: black - A_1^{CO}, green - A_2^{CO}, orange - A_3^{CO}, red - A_4^{CO} (see Table 2). The X-band ENDOR spectrum (A) was simulated using the hyperfine tensors determined from the Q-band ENDOR spectra. The signals, marked by asterisks are second harmonic of the ^{57}Fe signals.

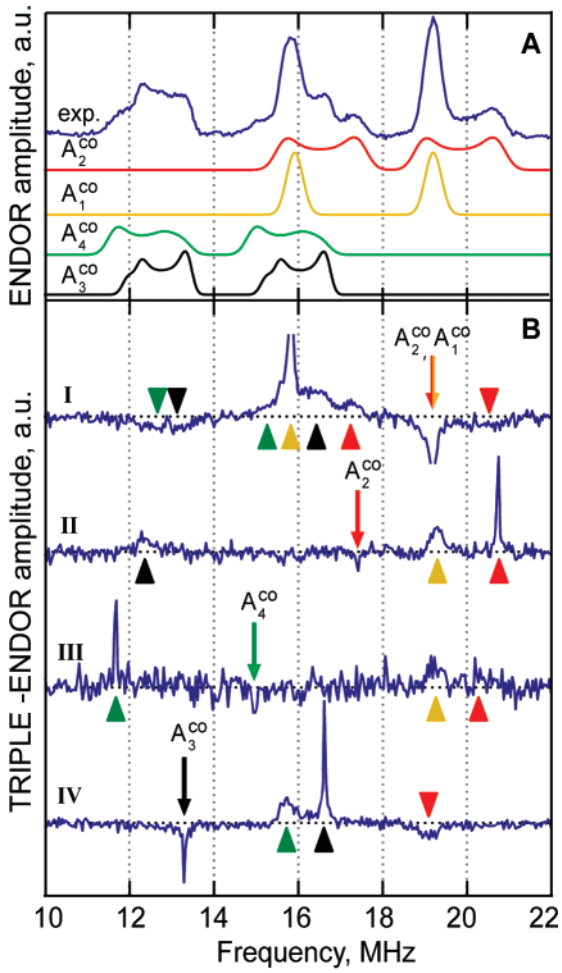

Figure 5. Q-band TRIPLE spectra of the ^{57}Fe-enriched H-cluster in the H_{ox}−CO state, taken at $g_2 = 2.007$. (A) Reference ENDOR spectrum with simulated components A_1^{CO}, A_2^{CO}, A_3^{CO}, A_4^{CO} from Table 2. (B) Difference (TRIPLE ENDOR) Q-band spectra for various pump frequencies (second RF pulse) at 19.19 MHz (I); 17.40 MHz (II); 15.00 MHz (III); 13.29 MHz (IV). The arrows in the plot indicate these frequencies. The color of the arrows corresponds to the HFI components of the ENDOR spectrum (panel A), which were predominantly excited. The triangles in B assign the peaks in the difference TRIPLE spectra to the hyperfine couplings of the ENDOR spectrum using the same color code as in A. Experimental conditions: microwave frequency, 33.884 GHz, temperature, 15 K; magnetic field, 1205.4 mT (g_2); length of the RF pulses, 45 μs; repetition time, 2 ms; shots per point, 50.

signal-to-noise (S/N) ratio but suffers from overlap with the ^{1}H-ENDOR signals (centered around 14.5 MHz). This nicely demonstrates the higher spectral resolution in the ENDOR spectra at Q-band frequency, in which the ^{1}H ENDOR signals are shifted to a higher frequency region ($\nu_H = 51.1$ MHz at 1200 mT).

In order to determine the relative signs of the ^{57}Fe hyperfine couplings TRIPLE experiments at Q-band were performed as shown in Figure 5B. Difference TRIPLE spectra show signals of nuclear transitions originating from the same electron spin manifold (M_S) as the transition excited by the pump RF frequency.[48] However, if the longitudinal electronic relaxation time is comparable with the duration of the pulse sequence, it is also possible to observe peaks in the difference spectra that belong to the nuclear transitions in the other electron spin manifold[60] (this is called "indirect" TRIPLE effect). However, these peaks have the opposite sign with respect to the "direct" TRIPLE effect. In Figure 5B the peaks that correspond to the direct TRIPLE effect have negative amplitude, whereas the peaks owing to the relaxation effects are positive.

Spectrum II in Figure 5B has been measured, while the pump RF frequency was tuned to a nuclear transition corresponding to the second nucleus (A_2^{CO}, see arrow). This spectrum reveals three positive peaks owing to the indirect TRIPLE effect. Two of them correspond to the high-frequency line of the A_1^{CO} and A_2^{CO} doublet, and one matches the low-frequency line of the A_3^{CO} doublet. This indicates that the hyperfine tensors A_1^{CO} and A_2^{CO} have opposite sign with respect to the A_3^{CO} tensor. The spectrum, which has been measured with the pumping RF

(60) Hofer, P. Entwicklung von Puls-ENDOR-Verfahren und Ihre Anwendung auf Polyazetylen. Doctoral thesis. University of Stuttgart, May 1988.

Table 2. Principal Values of the ^{57}Fe Hyperfine Tensor of the H-Cluster of [FeFe]-Hydrogenases

		D. desulfuricans[a]							*D. vulgaris*[b]		*C. pasteurianum* I[c]	*C. pasteurianum* II[d]
Fe site	hfc	$A_{x'}$	$A_{y'}$	$A_{z'}$	$\|A_{iso}\|$ (MHZ)	φ (deg)	θ (deg)	ψ (deg)	$A_{x'}$, $A_{y'}$, $A_{z'}$ (MHz)	$\|A_{iso}\|$ (MHz)	A (MHz)	A_{iso} (MHz)
H_{ox}-CO state												
Fe_1 (Fe_2)	A_1^{CO}	-35.4	-35.0	-30.4	33.6±0.15	90±90	185±2	-	-32.19		31.0	
									-38.35	33.8±2.7	33.0	-28.3±1.5
Fe_2 (Fe_1)	A_2^{CO}	-34.5	-38.4	-30.7	34.5±0.20	90±20	5±10	-	-30.95		34.0	
Fe_3 (Fe_4)	A_3^{CO}	+27.8	+21.8	+30.3	26.7±0.2	6±5	110±3	-	+31.50		31.0	
									+29.45	29.6±1.35	33.0	+25.3±1
Fe_4 (Fe_3)	A_4^{CO}	+26.7	+23.8	+30.2	27.0±0.2	76±10	-93±3	-	+27.94		34.0	
Fe_p	A_5^{CO}	-5.3	-4.5	-2.2	4.0±0.10	110±10	25±3	44±10	-6.85	6.85±2	5.8	-9.5
Fe_d	A_6^{CO}	±2.1	±2.1	∓1.7	0.8±0.10	-	30±5	90±10	0	0	-	0
H_{ox} state												
[4Fe-4S]	A_1^{ox}	+11.2	+10.4	+11.6	11.1±0.20	0	0	0	+8.5	8.5±0.9	9.5	+7.5
		-11.2	-10.4	-11.6	11.1±0.20	0	0	0	-8.5	8.5±0.9		-7.5
Fe_p	A_2^{ox}	±12.3	±11.3	±12.9	12.4±0.20	0	0	0	0	0	17±1	-
Fe_d		±12.3	±11.3	±12.9	12.4±0.20	0	0	0	-16.4	16.4±0.6		-18.0

[a] This work. The relative signs for the HF couplings were determined by TRIPLE experiments. The absolute signs were taken from Mössbauer data.[35,38] [b] Adapted from ref 35 (Mössbauer data). [c] Summary from ref 40 (ENDOR data). The authors did not assign the detected hyperfine couplings to the iron nuclei since the structure of the H-cluster was not known at that time. [d] Summary of refs 38,41 (ENDOR and Mössbauer data). Only isotropic values have been presented.

pulse simultaneously exciting spin transitions of the nuclei 1 and 2 (spectrum I), reveals triple difference peaks of both signs. Here the peaks of the spin transitions of nuclei 3 and 4 appear on the same side of the spectrum, which indicates that tensors A_3^{CO} and A_4^{CO} have the same sign.

According to this analysis the following (relative) signs were found:

$$\text{sign}(A_1^{CO}) = \text{sign}(A_2^{CO}) = -\text{sign}(A_3^{CO}) = -\text{sign}(A_4^{CO}) \quad (4)$$

The two additional TRIPLE spectra (III and IV) measured at different pumping RF frequencies confirm this conclusion. Previous Mössbauer studies on [FeFe]-hydrogenase II of *C. pasteurianum*[38] and *D. vulgaris* Hildenborough[35] have shown similar hyperfine coupling values (see Table 2).

Due to the small gyromagnetic ratio of the ^{57}Fe nucleus, the ENDOR technique is less sensitive to hyperfine interactions smaller than approximately 10 MHz. ESEEM and related techniques are, in contrast, very sensitive to hyperfine interactions that have a magnitude twice as large as the nuclear Larmor frequency ($A_{Fe} \approx 2\nu_{Fe}$), which is approximately 3.3 MHz for ^{57}Fe at 1.2 T (Q-band). In order to detect the smaller ^{57}Fe hyperfine couplings in the H_{ox}−CO state of the H-cluster, Q-band HYSCORE experiments were performed at the positions $g_1 = 2.065$ and $g_2 = 2.007$. Because of the broadening of the EPR spectrum by large ^{57}Fe hyperfine couplings (in this case features g_2 and g_3 are not resolved) and due to the hard MW pulses used for the HYSCORE sequence, it was assumed that all orientations along g_2 and g_3 are excited. The results are shown in Figure 6 A,C.

In the HYSCORE spectra cross-peaks belonging to nuclei with weak hyperfine coupling ($|A| < |2\nu_{Fe}|$) appear in the (+ +) quadrant, while strong hyperfine couplings ($|A| > |2\nu_{Fe}|$) show up in the (+ −) quadrant. Due to the "blind-spot" effect, ridges belonging to the strong hyperfine interaction appear with long τ values, while peaks corresponding to weak hyperfine interaction are more prominent in HYSCORE spectra with small τ (<350 ns). Here we present spectra, with $\tau = 352$ ns, which was found to be the optimum for simultaneous observation of both ridges. The HYSCORE spectra at the higher magnetic field position ($g_2 = 2.007$) reveal two ^{57}Fe hyperfine couplings: one cross-peak pair corresponding to a weak interaction in the (+ +) domain and one in the (+ −) domain, which corresponds to a relatively strong hyperfine interaction. The measurements at g_1 (low magnetic field) show only one ^{57}Fe ridge in the (+ +) quadrant, which belongs to the small hyperfine coupling. Simulations of these HYSCORE spectra (Figure 6B,D) were performed using parameters A_5^{CO} and A_6^{CO} from Table 2. Our calculations show that the intensity of the peaks corresponding to the ^{57}Fe nucleus with stronger hyperfine coupling for the g_1 position is smaller than those for peaks corresponding to the ^{57}Fe nucleus with the weak hyperfine coupling. This can be

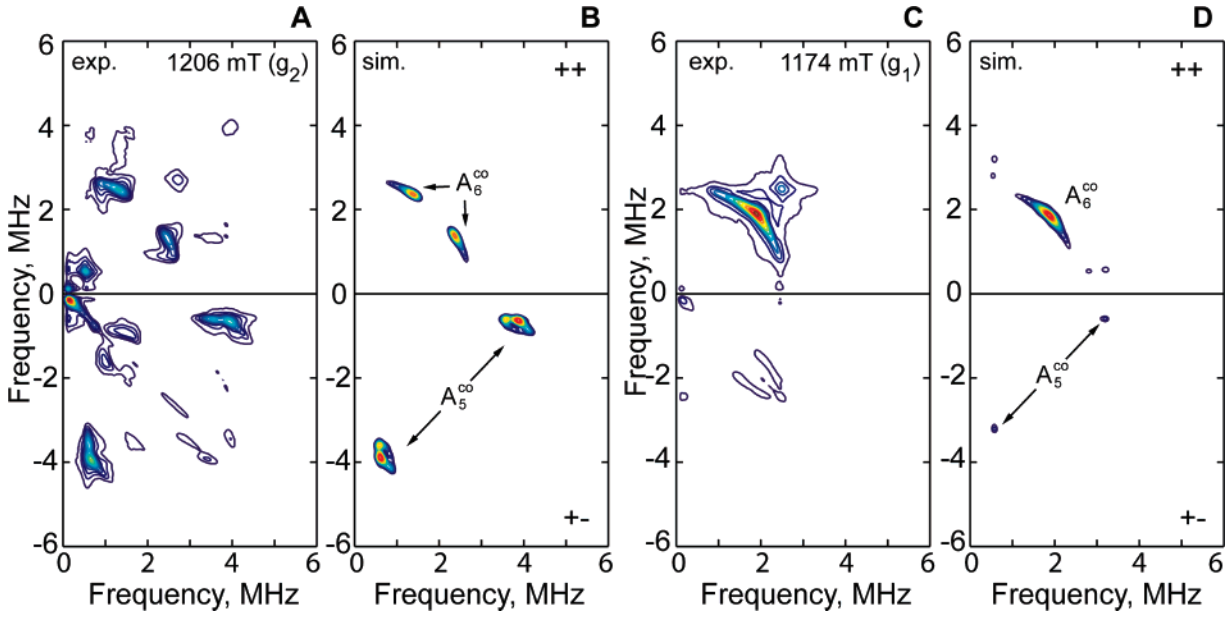

Figure 6. Q-band HYSCORE spectra of [FeFe]-hydrogenase of *D. desulfuricans* ^{57}Fe-enriched H-cluster in the H_{ox}−CO state at different magnetic field: (A) 1206 mT (g_2), (C) 1174 mT (close to g_1), and simulated spectra (B,D) using parameters A_5^{CO} and A_6^{CO} from Table 2. Experimental conditions: temperature, 20 K; length of all microwave pulses, 40 ns; delay between the first and second MW pulse (τ), 352 ns; microwave frequency, 33.884 GHz.

one of the reasons why we observe only one hyperfine coupling in the HYSCORE spectrum for the g_1 position. Additionally, the effect of suppression of cross-peaks of nuclei with small modulation depth in the presence of deep modulations, which was recently described by Stoll et al.,[61] could also explain our observations.

In addition to the ridges already mentioned above, the HYSCORE spectra of the ^{57}Fe-enriched H_{ox}−CO state show additional weak signals, which most probably originate from ^{14}N hyperfine couplings of the CN ligands and/or the N atom of the di(thiomethyl)amine of the binuclear subcluster and their combination frequencies. Earlier X-band ESEEM experiments on the [FeFe]-hydrogenase from *D. vulgaris* Hildenborough already showed signals attributed to ^{14}N hyperfine couplings.[62,63]

^{57}Fe Hyperfine Couplings of the H_{ox} State. ^{57}Fe ENDOR spectra at X- and Q-band measured for the H_{ox} state of the H-cluster in the range 1−10 MHz are shown in Figure 7. ENDOR measurements on the H_{ox} sample in the frequency range 10−20 MHz (not shown) revealed spectra, very similar to the ^{57}Fe ENDOR spectra of the H_{ox}−CO, presented in Figure 4. These peaks had a maximum intensity at a magnetic field around $g = 2$, which corresponds to the maximum of the EPR absorption line for the H_{ox}−CO state and vanishes with decreasing magnetic field. At $g = 2.1$ these peaks were not detectable at all, while the low-frequency peaks in the ENDOR spectrum are still present. Although it cannot be excluded that H_{ox} shows (weak) signals in this range, this seems unlikely since all observed features could be accounted for by using the H_{ox}−CO data. This observation confirms that the contaminating signal is due to a small fraction of the H_{ox}−CO species and thus supports the "cannibalization effect" discussed above.[29]

The low-frequency peaks (around 4 and 7.5 MHz) represent an ^{57}Fe hyperfine coupling of about 12 MHz (strong hyperfine coupling case). These peaks have not been observed in the H_{ox}−CO spectra and are therefore assigned to the H_{ox} species. The line shape of these peaks is, however, quite complex, and a detailed analysis indicates that the signal is due to at least two ^{57}Fe nuclei with hyperfine couplings of the same order of magnitude (see Table 2, A_1^{ox} and A_2^{ox}). Since the intensities of the two doublets differ by about a factor of 2, it can be assumed that they represent two sets of almost equivalent ^{57}Fe nuclei with a ratio of 2:1. The investigation of the H_{ox} state of the H-cluster by HYSCORE spectroscopy (spectra not shown) did not show any additional ^{57}Fe hyperfine couplings.

In order to determine the number of ^{57}Fe nuclei contributing to the ENDOR signal, we analyzed the lineshapes of the CW X-band EPR spectra of H_{ox} for the ^{57}Fe-enriched and the non-enriched ("native") protein. The line broadening effect caused by the ^{57}Fe enrichment is displayed in Figure 8 for the low-field ($g_1 = 2.10$) component of the EPR spectrum. The spectral simulations using an increasing number of interacting ^{57}Fe nuclei show that the best fit to the experimental spectrum is obtained with six interacting iron nuclei: four nuclei with hyperfine couplings described by the respective value of A_1^{ox} and two nuclei described by A_2^{ox} (see Table 2).

Discussion

Spin Coupling Model. The signs and magnitudes of the determined ^{57}Fe hyperfine couplings have been analyzed using a theoretical model which assumes that the unpaired spin residing on the binuclear subcluster $[2Fe]_H$ ($S = {}^1/_2$) is exchanged coupled through the cysteine thiolate bridge to one of the high-spin iron atoms of the diamagnetic $[4Fe{-}4S]^{2+}$ cluster.[35,38] The $[4Fe{-}4S]^{2+}$ cluster consists of two pairs of high-spin Fe^{II} and Fe^{III} centers. Each $Fe^{II}{-}Fe^{III}$ pair, with delocalized valences, in the cubane has a total spin of ${}^9/_2$.[64,65] The strong antiferromagnetic spin exchange coupling between the two pairs

(61) Stoll, S.; Calle, C.; Mitrikas, G.; Schweiger, A. *J. Magn. Reson.* **2005**, *177*, 93−101.
(62) Van Dam, P. J.; Reijerse, E. J.; Hagen, W. R. *Eur. J. Biochem.* **1997**, *248*, 355−361.
(63) Williams, R.; Cammack, R.; Hatchikian, E. C. *J. Chem. Soc., Faraday Trans.* **1993**, *89*, 2869−2872.

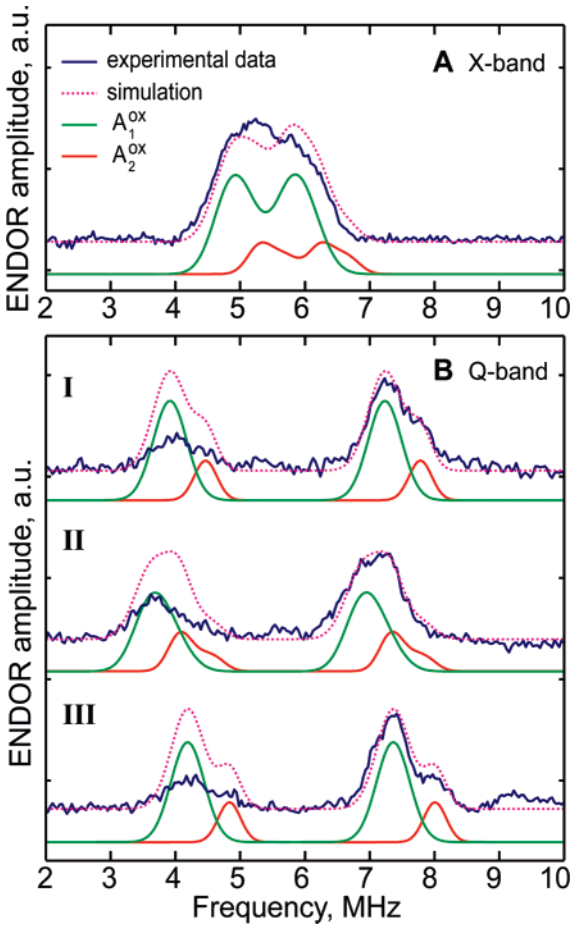

Figure 7. X- and Q-band Davies ENDOR spectra of ^{57}Fe-enriched [FeFe]-hydrogenase of *D. desulfuricans* in the H_{ox} state. (A) X-band Davies ENDOR spectrum, recorded using $t_{RF} = 10$ μs RF pulse; the magnetic field was set to 340 mT ($B_0||g_2 = 2.04$); microwave frequency, 9.74 GHz; temperature, 15 K. (B) Q-band ENDOR spectra. (I) 1153 mT (g_1) $t_{RF} =$ 110 μs; (II) 1186 mT (g_2), $t_{RF} = 110$ μs; (III) 1207 mT (g_3), $t_{RF} = 100$ μs; microwave frequency, 33.86 GHz, temperature, 15 K. The blue curves represent experimental data. The dotted magenta curves are the simulations of the ENDOR spectra using parameters A_1^{ox} and A_2^{ox} presented in Table 2. The HFI components of the individual ^{57}Fe nuclei are indicated with green lines (A_1^{ox}) and red lines (A_2^{ox}).

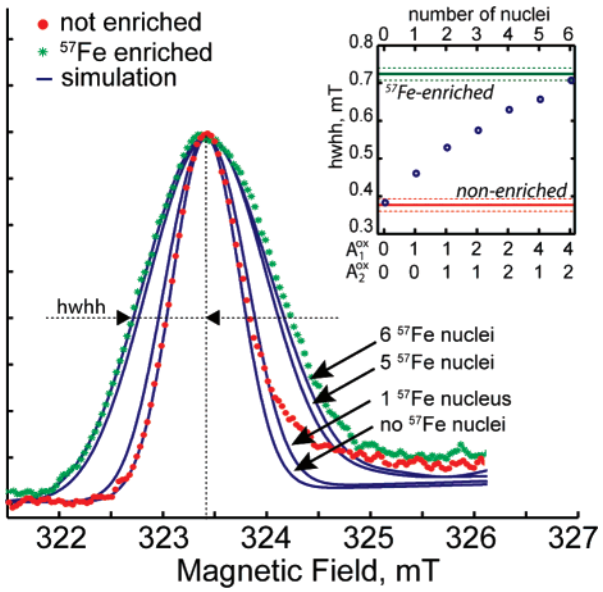

Figure 8. Broadening of the X-band H_{ox} EPR spectrum due to the presence of ^{57}Fe hyperfine interactions. The plot of the low-field component (g_1) of the X-band rhombic EPR spectra of nonenriched (red dots) and ^{57}Fe-enriched (green stars) [FeFe]-hydrogenase from *D. desulfuricans* in the H_{ox} state and simulation of these spectra assuming different numbers of ^{57}Fe nuclei (blue solid lines) with HFI taken from Table 2 (A_1^{ox} occurring up to 4 times and A_2^{ox} occurring up to two times). The plot in the inset represents the dependence of the half width at half-height (hwhh) of the low-field EPR component on the number of nuclei included in the simulation. The dashed lines represent the estimated uncertainty range in the determination of the line width. At the bottom of the inset, the number of nuclei with hyperfine couplings A_1^{ox} and A_2^{ox}, taken into account, are presented. Experimental conditions: temperature, 50 K; microwave power 20 μW; microwave frequency, 9.5968 GHz; modulation amplitude, 0.3 mT with 100 kHz modulation frequency; time constant, 40.96 ms, total scan time, 81 s.

leads to a $S = 0$ ground state (singlet) for the $[4Fe-4S]^{2+}$ cluster with an $S = 1$ excited state (triplet) at energy distance Δ. The additional exchange coupling (j) of the $[2Fe]_H$ cluster ($S = {}^1/_2$ center) to one of the iron atoms of the "cubane" cluster leads to a mixing of the ground (singlet) and first excited (triplet) states of the cubane (S−T mixing). The strength of this mixing and consequently the hyperfine coupling of the iron nuclei of the cubane depend on the ratio j/Δ. The model predicts that the signs of the hyperfine interactions corresponding to the two $Fe^{II}-Fe^{III}$ pairs are opposite. This is exactly what has been found for the large couplings observed in the H_{ox}−CO state (see Table 2) using TRIPLE experiments.

The model seems to describe the observed ^{57}Fe hyperfine couplings in the H_{ox} and H_{ox}−CO state quite well. For the H_{ox} state the mixing effect is rather small, leading to relatively small isotropic hyperfine couplings of the nuclei in the cubane and larger HF couplings of the $[2Fe]_H$ subcluster as compared to the H_{ox}−CO state. The H_{ox}−CO state is characterized by a strong S−T mixing (caused by an increased electronic exchange coupling j) leading to ^{57}Fe hyperfine couplings that are a factor of 3 larger than those of the H_{ox} state. Our observations indicate that the exchange-coupling model described above is basically correct but needs some refinements in order to fully describe the electronic structure of the H-cluster. For example, the model is not taking into account the presence of the distal iron of the binuclear subcluster, which apparently also carries some spin density. Furthermore, the fact that the four observed hyperfine couplings from the cubane are all different (at least in H_{ox}−CO) shows that the symmetry of the cubane is lower than D_{2d}, which was the starting assumption for the spin coupling model of the $[4Fe-4S]^{2+}$ cluster.[64]

Assignment of ^{57}Fe Hyperfine Tensors. For elucidating the spin density distribution of the H-cluster, a full assignment of the ^{57}Fe HF couplings is indispensable. For the H_{ox} state six ^{57}Fe couplings were assigned (see Table 2) by combination of ENDOR spectroscopy and EPR line shape analysis.[66] According to the coupling model discussed above, it is expected that four almost identical ^{57}Fe hyperfine couplings for the irons in the $[4Fe-4S]_H$ subcluster will be found. On the basis of this argument we suggest that the four hyperfine couplings (A_1^{ox}) are originating from the four iron nuclei in the cubane subcluster,

(64) Bominaar, E. L.; Hu, Z. G.; Münck, E.; Girerd, J. J.; Borshch, S. A. *J. Am. Chem. Soc.* **1995**, *117*, 6976−6989.
(65) Belinsky, M. I. *J. Biol. Inorg. Chem.* **1996**, *1*, 186−188.

(66) Lineshape analysis, in this case, provides only indirect evidence of HF coupling constants. Therefore, the case with four A_1^{ox} and one A_2^{ox} (Figure 8) cannot be completely excluded, although it seems unlikely. Further evidence for our assignment could be obtained from analysis of the spin density on the CO and CN ligands of the H-cluster.

while the two larger hyperfine couplings (A_2^{ox}) correspond to two iron nuclei in the binuclear subcluster $[2Fe]_H$. The Mössbauer spectra[35,38] were interpreted as caused by two sets of ^{57}Fe hyperfine couplings around 8 and 17 MHz. In our experiments these finding could not be confirmed, since no ENDOR signals were found in this frequency range. The frequency range was accessible and not contaminated with lines from the superimposed H_{ox}−CO species.

For the H_{ox}−CO state two rather small hyperfine couplings (A_5^{CO}, A_6^{CO} in Table 2) were found and assigned to the binuclear subcluster. According to the spin-coupling model the $[2Fe]_H$−$[4Fe{-}4S]_H$ exchange interaction is much larger in this state than that in the H_{ox}-state. Therefore, it seems likely that the larger of the two hyperfine couplings (A_5^{CO}) is associated with the proximal iron, which forms the connection to the $[4Fe{-}4S]_H$ subcluster, while the small hyperfine coupling (A_6^{CO}) then belongs to the distal iron.

The four large couplings have been assigned to the $[4Fe{-}4S]_H$ subcluster of the H-cluster in the H_{ox}−CO state (A_{1-4}^{CO}, see Table 2). It is not clear, which particular hyperfine coupling belongs to which iron in this subcluster, although some indication could be obtained from considering the orientations of the hyperfine tensors in the structure. Although the determined Euler angles are not very accurate, they do provide certain constraints, which allow us to relate the ^{57}Fe hyperfine tensor orientations to the crystal structure of the H-cluster in the H_{ox}−CO state.[17] It should be realized, however, that all angles are determined with respect to the principal axes of the **g** tensor.

Since the electronic structure of the H_{ox}−CO state is dominated by the strong exchange interaction between the binuclear subcluster and one of the iron atoms of the cubane subcluster, it is reasonable to assume that the vector connecting the subclusters represents a local symmetry axis defining the main principal direction of the **g** tensor, i.e., g_z. The orientations of the hyperfine interaction tensors can only be partially defined through our experimental analysis (see Table 2). In addition, there are several combinations of φ (rotation around *z*-axis) and θ (rotation around y' axis) which merely permute the order of the principal components; that is applying a rotation with $\varphi = 90°$ and $\theta = 90°$ results in a cyclic permutation of the principal axes. Finally, the small hyperfine coupling originating from the binuclear subcluster has axial symmetry, which allows additional rotational freedom around φ. On the other hand the orientation along the *z*-axis of the **g** tensor (θ) for each tensor can be determined quite accurately.

It was found that the *z* components of the hyperfine tensors of the cubane pair of irons with the largest hyperfine couplings (A_1^{CO} and A_2^{CO}) are almost collinear with each other and with the *z*-axis of the **g** tensor. At the same time, the "*z*" components of the ^{57}Fe hyperfine couplings of pair A_3^{CO}−A_4^{CO} appear to be oriented perpendicular to the other pair. All together, this suggests that the tensor orientations may follow the local symmetry of the cubane such that the "*z*" components of the hyperfine tensors are oriented along the diagonals connecting the iron pairs. There are three ways to combine four irons in the $[4Fe{-}4S]_H$ subcluster into two pairs. However, an additional restriction can be derived from the alignment of the hyperfine tensor of the proximal iron (A_5^{CO}). Because of the strong $[2Fe]_H$−$[4Fe{-}4S]_H$ exchange interaction, the *z*-axis of this tensor should be approximately along the Fe_p−S_{cys} bond, which

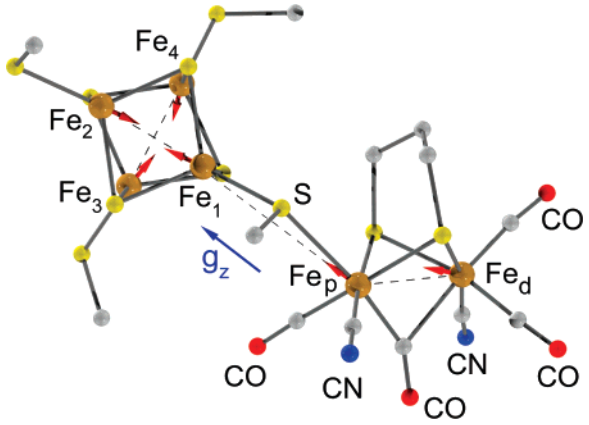

Figure 9. Schematic representation of the orientation of the ^{57}Fe hyperfine tensors in the structure of the H-cluster in the H_{ox}−CO state. The red arrows represent the local *z*-axis for each of the ^{57}Fe hyperfine tensors. Here we used the coordinates taken from the geometry-optimized structure of the H-cluster in the H_{ox}−CO state, presented by Fiedler et al.[27] The direction of the g_z component of the *g* tensor is also given. This picture was obtained using routines written in MatLab.[54]

is, in fact, in agreement with the recent DFT calculations.[44] Since this hyperfine tensor was determined with good accuracy (all three Euler angles were defined), its alignment can decrease the number of possibilities for the arrangement of the **g** tensor with respect to the molecular structure and therefore help in the assignment of the hyperfine tensors to the irons in the cubane. Combining all these arguments, we suggest that the pair of strong hyperfine couplings (A_1^{CO}−A_2^{CO}) is belonging to the Fe_1−Fe_2 pair and the pair of hyperfine tensors (A_3^{CO}−A_4^{CO}) to the Fe_3−Fe_4 pair. The tensor axis system (*z*-components) is given in Figure 9. The obtained data on the ^{57}Fe hyperfine interaction tensors will provide an important basis for future quantum chemical calculations on the H-cluster.

Effect of the External CO Ligand. Our results suggests that for the H_{ox} state the unpaired spin is distributed almost equally over the two iron atoms in the binuclear cluster while in the H_{ox}−CO state, the unpaired spin is shifted toward the proximal iron. The weak almost dipolar ^{57}Fe hyperfine coupling attributed to the distal iron seems to support the view that the spin density is strongly localized on the proximal iron in the H_{ox}−CO state. A similar trend upon binding of the external CO ligand is observed in the recent theoretical calculations by Fiedler et al.[44] These authors used the geometry optimized coordinates obtained from a calculation including both $[2Fe]_H$ and $[4Fe{-}4S]_H$ subclusters to obtain the properties of the singly occupied orbital (SOMO) localized on the binuclear cluster. These calculations, however, suggest that in the H_{ox} state most of the unpaired spin density is localized at the distal iron, while in the H_{ox}−CO state it is redistributed over the binuclear subcluster. Placing an additional CO ligand at the distal iron leads to an increase of the Fe_p−Fe_d distances from 2.56 Å for H_{ox} to 2.71 Å for H_{ox}−CO, as well as a shift of the bridging CO ligand toward the proximal iron. Addition of the external CO ligand weakens the coupling between the two iron atoms and leads to a stronger localization on the spin density, in this case at the proximal iron. This, in turn, increases the exchange interaction between the unpaired spin in the binuclear subcluster with the cubane as is observed experimentally. The predicted shift of effective spin density toward the $[4Fe{-}4S]_H$ subcluster upon binding of the CO ligand is confirmed by our experiments. However, as

the authors noticed, the calculated ^{57}Fe hyperfine interactions of the $[2Fe]_H$ subcluster do not match the experimental ones very well.[44] In particular, the calculated anisotropy of the hyperfine tensors is too large. Popescu and Münck[38] have argued that in case of a Fe^IFe^{II} configuration in the H_{ox} and H_{ox}−CO state the unpaired electron would be in an e_g orbital producing a substantial dipolar term in the hyperfine interaction. Indeed, the tensor values obtained in our experiments do show a 1−2 MHz anisotropy which is, however, much smaller than that calculated by Fiedler et al.[44] Apparently, the covalent coupling to the [4Fe−4S] cluster has a profound effect on the structure of the SOMO. The fact that the calculated ^{57}Fe hyperfine values are very sensitive to the protonation state of the bridging cysteine illustrates this effect.[44]

Iron Redox States of the Binuclear Subcluster. In the literature there is still some debate about the possible redox states of the binuclear iron cluster in the various catalytic states. Inorganic model systems of the binuclear subcluster have been prepared[67] which show that in the completely reduced state the Fe^IFe^I arrangement is very stable. These findings have also been confirmed by quantum chemical calculations.[42,68] On the other hand, the Mössbauer studies on the H-cluster suggest a $Fe^{II}Fe^{II}$ arrangement for the reduced state although a Fe^IFe^I configuration could not be completely ruled out.[35] The current data clearly indicate that the proximal iron atom must be formally paramagnetic in order to give rise to the extensive electron exchange interaction with the cubane subcluster. At the same time, IR studies[29,36] have shown that the frequency of the CO stretch vibration of the CO bound to the proximal iron (Fe_p) is not changing when the state of the H-cluster is changed, i.e., it remains at 1964 cm^{-1} in the H_{ox} and the H_{red} state as well as the H_{ox}−CO state. This indicates that the redox transition occurs at the distal iron Fe_d when going from the H_{ox} to the H_{red} state. This would make sense if the reaction with molecular hydrogen were initiated at the open coordination site, which is at Fe_d. Both irons in the $[2Fe]_H$ subcluster are in the low-spin state,[38] which is caused by the strong ligand field (CN^-, CO ligation). It is known that Fe^{II} in the low-spin state is diamagnetic whereas Fe^I and Fe^{III} are paramagnetic. Since the proximal iron is paramagnetic in H_{ox} and H_{ox}−CO, its redox state can only be Fe^I. If it were to be be in the Fe^{III} state, the reduction of the H-cluster would have to take place at the proximal iron and change the redox state which would be inconsistent with the infrared data. Therefore, the combination of data from ENDOR, HYSCORE, Mössbauer, and IR allows us to conclude that during the catalytic cycle the binuclear subcluster shuttles between the $Fe^I_pFe^I_d$ and $Fe^I_pFe^{II}_d$ state. Therefore, on the basis of our results, we incline to the general catalytic scheme that was proposed recently[9] (outlined in Figure 10).

Comparison with Earlier Investigations. In Table 2 the results of our Q-band ENDOR and HYSCORE measurements are compared with those obtained from previous ENDOR and Mössbauer experiments on the hydrogenases from *D. vulgaris* and *C. pasteurianum*.[35,38,40,41] For the H_{ox}−CO species the correspondence is quite satisfactory. Both *D. vulgaris* and *C. pasteurianum* hydrogenases show strong ^{57}Fe couplings, which are assigned to the cubane subcluster. The obtained hyperfine

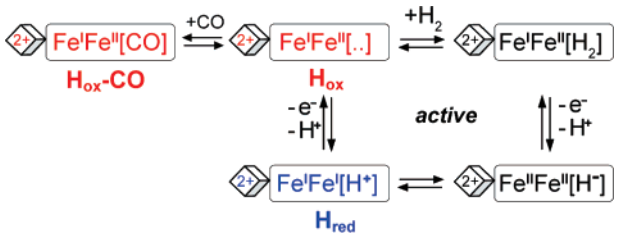

Figure 10. Generalized scheme of the catalytic mechanism of the [FeFe]-hydrogenase, including the oxidation level of the $[4Fe-4S]_H$ subcluster (indicated as ◇), the individual oxidation states of the irons in the $[2Fe]_H$ cluster, and the occupancy of the open coordination site at the Fe_d (in square brackets). Redox transitions ($1e^-$) are shown (vertical) as well as the proposed catalytic cycle and the inhibition of the enzyme by CO.

coupling values are very close to the ones we have found for *D. desulfuricans* H_{ox}−CO. Some differences are apparent when comparing the couplings assigned to the binuclear subcluster. While the data for *D. vulgaris* and *C. pasteurianum* hydrogenase suggest a singular isotropic coupling in the range 6−9 MHz (see Table 2), we find two somewhat smaller couplings with substantial anisotropy using HYSCORE spectroscopy. The general picture of the spin density distribution remains, however, the same in both the ENDOR/HYSCORE on the *D. desulfuricans* and the Mössbauer/ENDOR studies on *C. pasteurianum* hydrogenase and *D. vulgaris*.

A different situation occurs when comparing our results on the H_{ox} species with those of the earlier Mössbauer and ENDOR studies. While the latter studies result in two ^{57}Fe hyperfine couplings, which differ by a factor of 2 (8.5 and 16.4 MHz), we found two quite similar hyperfine couplings (isotropic values of 11.1 and 12.4 MHz). The 16.4 MHz coupling (Mössbauer on *D. vulgaris*) was assigned to the distal iron in the binuclear subcluster. On the basis of the intensity ratio of the peaks in the ENDOR spectra of the two couplings we also assign our largest coupling (12.3 MHz) to the binuclear subcluster. It should be noted that the Mössbauer spectra are difficult to analyze due to the many parameters involved as well as the large number of overlapping signals (overall 14 iron nuclei, *D. vulgaris*). The original ENDOR studies of hydrogenases I and II from *C. pasteurianum* by Telser et al.,[40,41] however, did not suffer from these problems, and the obtained values of the hyperfine couplings should be regarded as reliable. Therefore, on the basis of our experimental data, it cannot be excluded that the electronic structure of the H-cluster in the hydrogenases from *C. pasteurianum* differs from that in *D. desulfuricans*.[69,70]

Conclusions

The combined application of different hyperfine resolving techniques at two different microwave frequencies enabled us to determine a complete set of ^{57}Fe hyperfine tensor values for the hydrogen activating unit (H-cluster) of [FeFe]-hydrogenase

(67) George, S. J.; Cui, Z.; Razavet, M.; Pickett, C. J. *Chem. Eur. J.* **2002**, *8*, 4037−4046.
(68) Darensbourg, M. Y.; Lyon, E. J.; Zhao, X.; Georgakaki, I. P. *Proc. Natl. Acad. Sci. U.S.A.* **2003**, *100*, 3683−3688.
(69) It should be noted that the most detailed ENDOR and Mössbauer experiments have been performed on hydrogenase II from *C. pasteurianum* of which no crystal structure is available. Up to now, however, no follow-up studies of any kind have been published on hydrogenase II. Also, we were not able to find a gene encoding for this hydrogenase in the genome databases (e.g., UNI-PROT). Therefore, it cannot be completely excluded that hydrogenase II is an artifact, e.g. a partly denatured hydrogenase I enzyme. Since in the meantime hydrogenase I of *C. pasteurianum* has been characterized very well, it may be worthwhile to repeat the ENDOR and Mössbauer experiments on this enzyme to verify the reported ^{57}Fe hyperfine values.
(70) Kowal, A. T.; Adams, M. W. W.; Johnson, M. K. *J. Biol. Chem.* **1989**, *264*, 4342−4348.

in the paramagnetic states H_{ox} and H_{ox}−CO of the ^{57}Fe-labeled enzyme. A total of six ^{57}Fe hyperfine couplings is found for both the active oxidized and the CO-inhibited state. This is an important finding since the oxidized $[4Fe-4S]^{2+}$ subcluster should formally be diamagnetic only if the $[2Fe]_H$ subcluster is EPR-active in the mixed-valent state. The experimental data show that the unpaired spin density distribution is extending over the entire H-cluster. This finding supports the exchange-coupling model proposed earlier to explain the Mössbauer experiments on the H-cluster.[38] In this model the observation of ^{57}Fe hyperfine couplings from the cubane in both states H_{ox} and H_{ox}−CO is caused by a strong spin exchange coupling between the two subclusters giving rise to a rather large "indirect" spin density at the cubane. The measured relative signs of the ^{57}Fe hyperfine tensor components assigned to the cubane irons confirm this interpretation.

The electronic structures of the H_{ox} and H_{ox}−CO state are clearly different. Binding of the external CO at the free coordination site at the distal iron Fe_d shifts spin density toward the proximal iron and strongly increases the spin exchange coupling between the two subclusters leading to a stronger "apparent" spin density at the cubane and a weaker spin density at the $[2Fe]_H$ subcluster. The pairwise valence delocalized Fe^{II}-Fe^{III} arrangement in the cubane subcluster is in line with the orientation of the main ^{57}Fe hyperfine axes deduced from the orientation-selective ^{57}Fe Q-band ENDOR experiments.

On the basis of the EPR/ENDOR, Mössbauer,[35,38] and IR[25,36] data the formal oxidation states of the two irons in the binuclear subcluster could be deduced. It has been shown that no Fe^{III} is present in the $[2Fe]_H$ subcluster. The proximal iron (Fe_p) remains in the +1 state in H_{ox} and H_{red}, and the distal iron (Fe_d) alternates between the +2 (ox) and +1 (red) state. This assignment leads to a general catalytic scheme for the H-cluster in the [FeFe]-hydrogenase, which could describe both the H_2 splitting and production. In this cycle dihydrogen is heterolytically split at the distal iron (H_2 uptake), with the hydride intermediate remaining at the Fe_d. In the inhibited H_{ox}−CO state this position is blocked by the external CO ligand. A detailed mechanism of the H_2 splitting process also requires knowledge of the fate of the proton, which is probably initially attached to a nearby base before disposal via the proton-transfer channel. Such a base could be provided by the nitrogen in the di(thiomethyl)amine ligand that has been proposed to bridge the two iron atoms in the binuclear subcluster.[28] Experiments to finally decide on the presence of nitrogen in this ligand using magnetic resonance techniques are underway in our laboratory.

Another point of interest is the function of the CO and CN^- ligands in the active center of the [FeFe]-hydrogenase. These ligands help to adjust the electronic properties of the metal center for the binding and heterolytic splitting—or the formation—of the dihydrogen. The electronic coupling of these ligands to the metal centers can be investigated by isotopic labeling (^{13}C, ^{17}O, ^{15}N) of the ligands and the determination of the respective nuclear hyperfine interaction tensors. In this context the photolability of the CO binding to the [FeFe] center is worth mentioning. It leads to scrambling of CO ligands under illumination of this hydrogenase.[29,36] Furthermore, the proposed opening of the CO bridge in the reduced state[28,71] is also highly interesting. This might point to a different mechanism of hydrogen conversion, in which a bridging hydride is formed in the intermediate reduced state of the enzyme quite similar to that found in [NiFe]-hydrogenase.[9,72−75] This interpretation, however, would contradict our current model, which identifies the distal iron as the primary binding site of dihydrogen. Alternatively, the bridge opening might point to the binding of a second dihydrogen (e.g., to the proximal iron) during the catalytic cycle as discussed by van Haaster et al.[76]

Finally, differences and similarities between the hydrogenases from different organisms are important to elucidate. We have, for example, discussed in this work that the [FeFe]-hydrogenases from *C. pasteurianum* most probably have a slightly different electronic structure from that of *D. desulfuricans*. Although the H-cluster in this class of enzymes seems to be structurally well conserved, subtle differences in protein ligation (H-bonding) of the H-cluster may lead to distinct differences in electronic structure which may have effects on the activity/directionality of the enzyme. Detailed knowledge of the factors which affect the electronic structure of the H-cluster would be of great importance also for the construction of bioinspired artificial hydrogenase catalysts.

Acknowledgment. Dr. C. Fichtner and D. Johansson are gratefully acknowledged for isolating the protein and providing samples of nonenriched [FeFe]-hydrogenase from *D. desulfuricans*, W. Roseboom for preparing the samples of the ^{57}Fe-enriched enzyme in the different states, Dr. B. Epel for providing support with the SpecMan software, and G. Klihm for technical assistance with the measurements. This project has been supported by the DFG priority program SPP1051, the Max Planck Society, and the EU (Solar-H 516510).

JA072592S

(71) Bruschi, M.; Fantucci, P.; De Gioia, L. *Inorg. Chem.* **2004**, *43*, 3733−3741.
(72) Brecht, M.; van Gastel, M.; Buhrke, T.; Friedrich, B.; Lubitz, W. *J. Am. Chem. Soc.* **2003**, *125*, 13075−13083.
(73) Foerster, S.; van Gastel, M.; Brecht, M.; Lubitz, W. *J. Biol. Inorg. Chem.* **2005**, *10*, 51−62.
(74) Stein, M.; Lubitz, W. *J. Inorg. Biochem.* **2004**, *98*, 862−877.
(75) Morris, R. H. Hydrogenases and Model Complexes. In *Concepts and Models in Bioinorganic Chemistry*; Kraatz, H.-B., Metzler-Nolte, N., Eds.; Wiley-VCH Verlag GmbH: Weinheim, 2006; pp 331−362.
(76) van Haaster, D. J.; Jongejan, J. A.; Hagedoorn, P. L.; Hagen, W. R. *Int. J. Hydrogen Energy* **2006**, *31*, 1432−1438.